International Journal of Chemistry, Mathematics and Physics (IJCMP)
[Vol-5, Issue-6, Nov-Dec, 2021]
https://dx.doi.org/10.22161/ijcmp.5.6.2
ISSN: 2456-866X

Cation distribution of Ni^{2+} and Mg^{2+} ions improve structure and Magnetic Properties of Spinel Ferrites

Pranali K. Tembhurne[1], Shrikant M Suryawanshi[2], Kishor G. Rewatkar[3], Dilip S. Chaudhary[4], Sanjay J. Dhoble[5]

[1]Gramgeeta Mahavidyalaya, Chimur, India
[2]Kamala Neharu Mahavidyalaya, Nagpur, India
[3]Dr.Ambedakar College, Nagpur, India
[4]Dhote Bandu Science College, Nagpur, India
[5]Department of Physics, Nagpur, India

Received: 09 Oct 2021; Received in revised form: 13 Nov 2021; Accepted: 21 Nov 2021; Available online: 30 Nov 2021

Abstract— *In the present work, ferromagnetic Ni is slightly substituted for diamagnetic Mg spinal ferrites. The effect of Ni doping on the structural and magnetic properties of ferrites material in the form of* $Ni_xMg_{1-x}Fe_2O_4$ *(x = 0.1,0.15,0.2,0.25, .0.3,0.35) has been the study. The Sol-gel auto Combustion method used to combine these substances uses urea as fuel. Sintered samples were shown using X-ray diffraction, Fourier Transform Infrared spectroscopy (FTIR) and a vibrating magnetometer sample. X-ray diffraction revealed that all the composite samples were pure cubic spinel arrays with a Fd3m space band and a permanent lattice that varied with Ni concentrations. the distribution of* Ni^{2+} *ions and* Mg^{2+} *ions in spinel ferrites indicates various changes in parameters such as tetrahedral ionic radius (*r_A*), octahedral ionic radius (*r_B*), hopping length (*L_A *and* L_B*). Fourier Transform Infrared (FT-IR) simulations showed wire vibration at the tetrahedral site and Octahedral site. spinel ferrites M-H curves are recorded at room temperature indicating normal hysteresis loop indicating the magnetic field.*

Keywords— ***Cation distribution, Magnetic Properties, Spinel Ferrites, nanobiotechnology, X-ray diffraction.***

I. INTRODUCTION

In recent years, a combination of magnetic nanomaterials has been investigated for use in a wide range of applications from radio frequencies to microwave frequencies [1,2].

Over the past decade, nanobiotechnology has attracted a lot of attention because of its therapeutic potential in various biomedical systems. The therapeutic potential of nanoparticles in biomedical applications is due to their unique physical and chemical properties such as nanometer size, large area to volume ratio, high bioavailability, interaction in cell space and cell membranes. Spinel ferrites are often exploited as technology; Their biomedical systems have attracted a lot of attention recently [3]. Physical, Chemical and Optical structures can be modified by magnetic doping (Co^{2+}, Mn^{2+}, etc.), zero-magnetic (Zn^{2+}, Cd^{2+}, etc.) and paramagnetic (Mg^{2+}, Al^{2+}, etc.) cations on spinel ceramic ferrites, more importantly introducing the concept of flexible magnetic structures. Changes in Property are due to the distribution of divalent and trivalent cations between the available tetrahedral (A) and octahedral (B) so-called exchange interactions [4,5]. Common formulas of spinel ferrites MFe_2O_4. where M is usually a transition metal or a combination of switching metals with the Fd3m space group. The strongest interaction between cation is the interaction between cation at sites A and B, so-called A-B connections, where the angle of the cation-anion-cation bond is 180 degrees. The second strongest interaction between cations at B sites, called B-B interactions [6].

In the current context, the interaction between $Ni^{2+}$and Mg^{2+} cations at octahedral and tetrahedral sites alter features such as magnetic, physical, and structural

properties. In particular, sol-gel method is an efficient technique which can be used to control microstructure, grain size and distribution of defects of samples [7].The substitution of Ni^{2+} to Magnesium spinel ferrites shows the good chemical stability, large magnetic anisotropy, moderate saturation magnetization, significant chemical stability and mechanical hardness[8].

II. RESULTS AND DISCUSSION

2.1 X-Ray Diffraction

X-ray diffraction pattern of annealed powder for $Ni_xMg_{1-x}Fe_20_4$. (x=0.1,0.15,0.2,0.25,0.3,0.35).covered by Sol-gel auto combustion method as shown in Fig.1. Stack graph of the XRD patterns show a wide range of sharp peaks such as (111), (220), (311), (400), (422), (511), and (440) that confirm the formation of a single-phase cubic spinel structure. There is no secondary or remaining phase appears in patterns that reflect its purity and luster The lattice constant (a) is calculated using $a = d (h^2 + k^2 + l^2)^{1/2}$. The size of the crystallite is calculated from the X-ray linear diffusion height (311) using the well-known Debye – Scherrer relationship. The average lattice constant values are estimated between 8.3933 and 8.3837 Å.

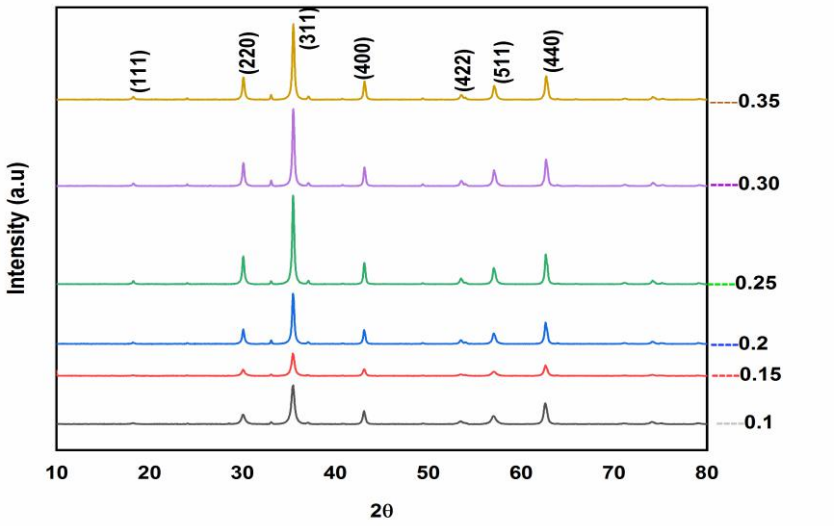

Fig.1 X-ray diffraction pattern of $Ni_xMg_{1-x}Fe_2O_4$(x=0.1,0.15,0.2,0.25,0.3,0.35)

The lattice value is constantly decreasing, this is due to differences in ionic radii of Ni^{2+} (0.069 nm) and Mg^{2+} (0.072 nm) and the size of the crystallite rises from x = 0.1 to x = 0.25 and then decreases from x = 0.3 to x = 0.35 are shown in Table 1. This difference in crystal size is due to the difference in energy between the metal-oxygen bond (low energy) and Fe-oxygen

bonds (high energy) and gravity affecting the crystal growth rate and crystal size [9,10]. The value of strain and dislocation density decrease with increasing Ni^{2+}ion as shown in table which indicates the. concentration of lattice imperfections, is decreases

The strain and dislocation density generated in the nanocrystals is computerized with the help of a relay.

$$\varepsilon = \frac{\beta}{4\tan\theta} \qquad 1$$

$$\delta = \frac{1}{d^2} \qquad 2$$

The distance between the magnetic ions called hopping lengths at the tetrahedral (A) site and the octahedral (B) site of all samples was assessed using lattice constant values for the following calculation

$$L_A = a * \frac{\sqrt{3}}{4} \qquad 3$$

$$L_B = a * \frac{\sqrt{2}}{4} \qquad 4$$

Table1: Different parameters lattice constants(a), crystalline size(D) ,strain(ε), dislocation constant(δ) ,hoping length (L_A) and (L_B) calculated by X-ray diffraction .

Composition (x)	a(Å)	Crystalline size (D)	Strain(ε)	Dislocation constant(δ)	L_A(Å)	L_B(Å)
0.1	8.3933	23.2696	$7.93x10^{-3}$	$1.85x10^{-3}$	3.6342	2.9670
0.15	8.3927	23.6373	$6.11x10^{-3}$	$1.78x10^{-3}$	3.6340	2.9668
0.2	8.3897	26.9346		$1.38x10^{-3}$	3.6327	2.9657
0.25	8.3884	32.0068	$4.83x10^{-3}$	$0.976x10^{-3}$	3.6321	2.9652
0.3	8.384	31.1036	$5.71x10^{-3}$	$1.03x10^{-3}$	3.6302	2.9637
0.35	8.3837	27.7557	$5.88x10^{-3}$	$1.29x10^{-3}$	3.6301	2.9636

2.2 Transmission Electron Microscopy (TEM)

TEM images with high resolution of Ni-Mg spinel ferrite samples as shown in Fig2a. and Fig2b. Particle size and microstructure of nanocrystalline Ni-Mg Spinel ferrite nanoparticles are identified by transmission electron microscope (TEM). In all micrographs it is evident that some particles are slightly agglomerated and complete agglomeration appears in a few particles, thus making them look like larger particles this is due to their magnetic nature.Particle size distributions of Ni^{2+} substituted magnesium spinel ferrites are shown in Fig 2a and Fig2b The histograms depict the size distribution of the particles, the average crystallite size is found nearly the same which is obtained from TEM micrographs and with the values obtained from the XRD analysis[11].The nanoparticles exhibited well separated continuous rings when analyzed by electron diffraction, SAED. The maximum diffraction intensity was found for (311) plan, consistent with the XRD pattern as shown by Fig 3.

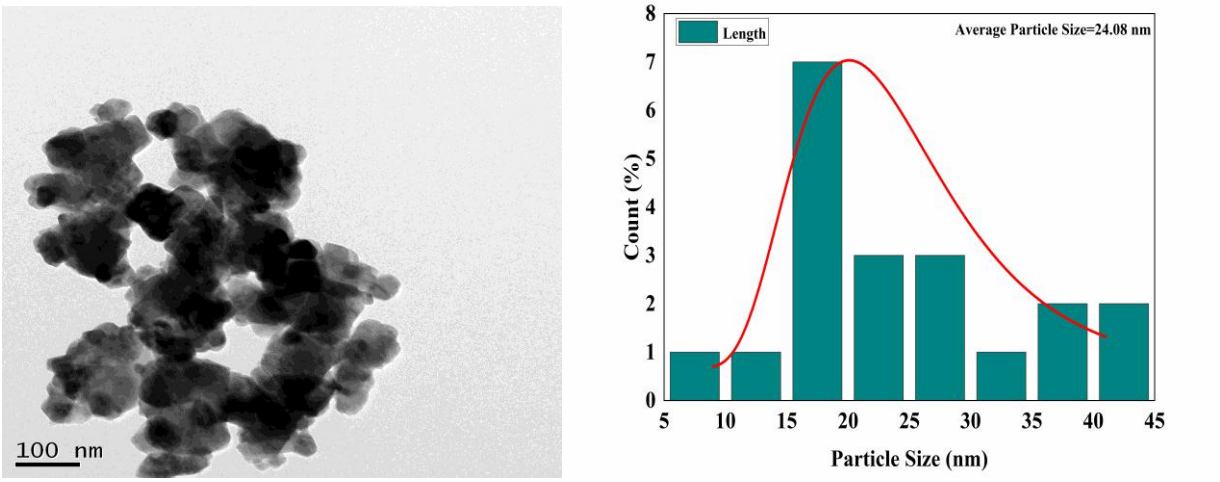

Fig 2a. TEM image and Histogram of $Ni_{0.1}Mg_{0.9}Fe_2O_4$

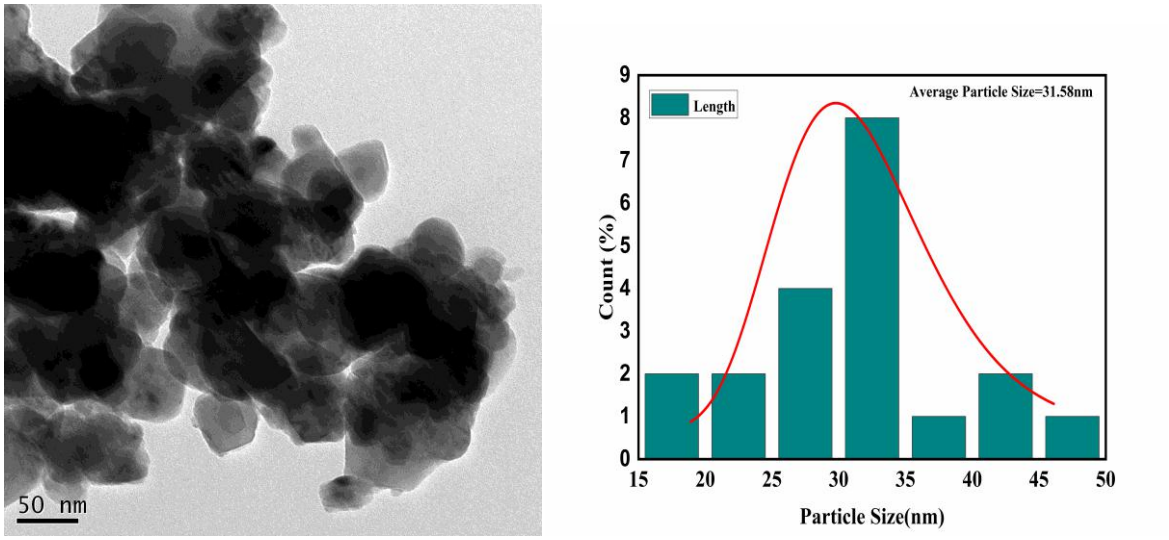

Fig2b. TEM image and Histogram of $Ni_{0.2}Mg_{0.8}Fe_2O_4$

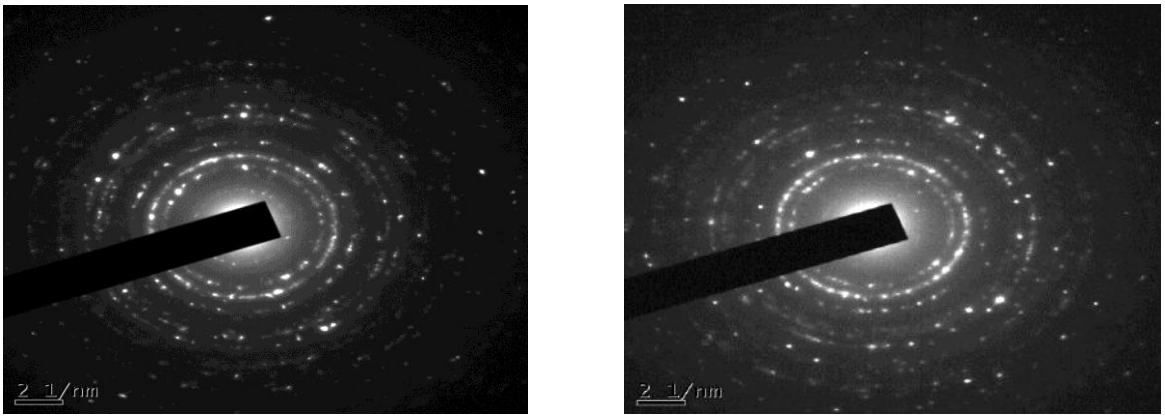

Fig 3. SAED Pattern of Ni doped Magnesium Ferrites (x=0.1,0.2)

2.3 Fourier Transform Infrared Spectroscopy (FTIR)

The structure of the $Ni_xMg_{1-x}Fe_20_4$ spinel structure (x = 0.1,0.2,0.3) confirms the FTIR spectra. All FTIR features are performed at room temperature within a range of wavelengths of 4000–400 cm^{-1}.Typically, a high-frequency band is seen at 600-500 cm^{-1}, accompanied by A-site vibration [$M_{tetra} \rightarrow O$] and a low-frequency band seen at a range of 500–400 cm^{-1},due to vibration of B-site groups [$M_{octa} \rightarrow O$], these two bands are common to all ferrites [13,14]. Notably, the bands are said to be at frequency 408.93cm^{-1}, 455.22 cm^{-1} and 462.94 cm^{-1} specified by (v_1) and the frequency range 601.82 cm^{-1}, 671.26cm^{-1} and 663.54cm^{-1} specified is (v_2) in the case of x = 0.1,0.2,0.3 as shown in **fig4.**

Table 2. Vibration band frequencies ($v_1$and v_2), force constant (K_t and K_0)and Tetrahedral(r_A)and Octahedral(r_B) site radii of the system $Ni_x\ Mg_{1-x}Fe_2O_4$ (for x = 0.1, 0.2 and 0.3)

x	v_1(cm^{-1})	v_2(cm^{-1})	K_t(dyne/cm)	K_o(dyne/cm)	Tetrahedral site radii(r_A)	Octahedral site radii(r_B)
0.1	601.83	408.93	2.654	1.225	0.4661	0.7483
0.2	671.26	455.22	3.302	1.518	0.4653	0.7474
0.3	663.4	462.93	3.225	1.57	0.4641	0.746

The frequency of the vibration band and the force constant depend on each other. The force constant can be calculated for tetrahedral site K_t and octahedral site K_o using the method suggested by Waldron [12]. The values of force constants K_t and K_o are listed in Table 2. It can be seen that both K_t and K_o are increasing with increasing Ni^{2+} content. Moreover, the fact that the calculated values of K_t are greater than those of K_o is due to the difference in the bondlength of the A-site r_A smaller than that of the B-site r_B are tabulated in Table2. The increase in force constants with increasing Ni^{2+} content suggests the strengthening of inter atomic bonding.

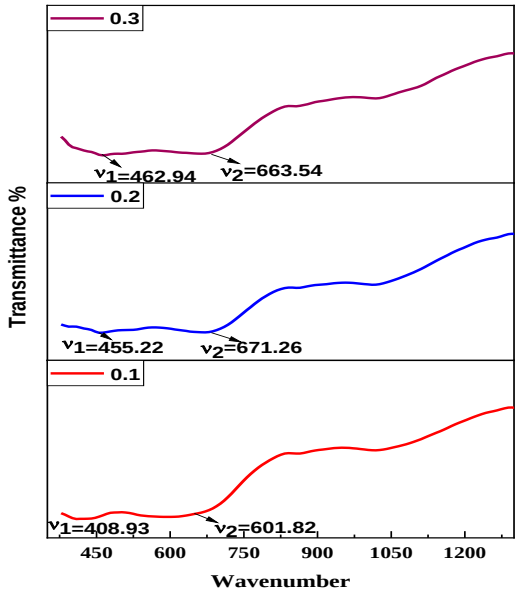

Fig. 4 Expanded view of FTIR spectra of $Ni_xMg_{1-x}Fe_2O_4$ (x=0.1,0.2, 0.3)

2.4 Vibrating Sample Magnetometer (VSM)

Magnetic properties of ferrites are characterized by a hysteresis loop. The magnetic properties of the combined nanoparticles of $Ni_xMg_{1-x}Fe_2O_4$ (x = 0.1,0.15,0.2,0.25,0.3,0.35) are measured at room temperature by vibrating the Magnet Sample on the applied field from - 20k Oe to + 20kOe. The saturation magnetization (Ms),Retentivity (Mr), and Coercivity (Hc) are taken from the hysteresis curve and their value is shown in Table 3. Sampling pressure increases non-monotonically, this is due to the distribution of Mg^{2+} and Ni^{2+} ions, inside.infectious diseases, anisotropy. The saturation magnetization (Ms) is increased by replacing Ni^{2+} ions. The increase in Ms. is due to strong interaction due to the replacement of Ni^{2+} magnetic ions with non-magnetic ferrites in Magnesium. The Mr / Ms rating is known as the SQR rating, its value is given in Table 3, the SQRs of the given system is 0.13 to 0.21 respectively. small numbers of loop squareness ratio indicate the presence of multiple domain particles in all compounds [13].

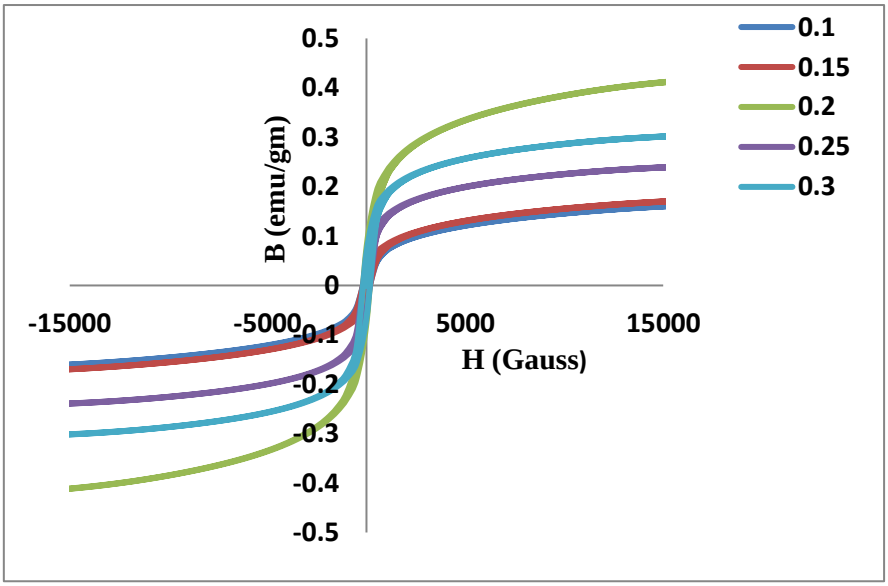

Fig.5 M-H loops for Ni substituted Magnesium Spinel ferrites ($Ni_xMg_{1-x}Fe_2O_4$)(x=0.1,0.15,0.2,0.25,0.3,0.35)

The magnetocrystalline anisotropy constant (K) of Ni-Mg spinel ferrites is measured by equation.

$$K = \frac{H_c M_s}{0.98} \qquad 5$$

The value of Hc depends on K, so with the increase of Ni2+ it prefers to octahedral B site,so increase K. The hysteresis curves show approximately zero coercivity and its value exhibit in the table reveals the nanocrystalline nature of the sample[14]. The magnetic properties of cubic spinel ferrites dramatically changes on account of a super exchange interaction mechanism occurring between the metal ions in the A and B sub-lattices.The Ni^{2+} ions occupy octahedral sites and Fe^{3+} ions are equally distributed in tetrahedral and octahedral sites, and Mg^{2+} ion gives strong preference to octahedral site compare to tetrahedral site and Ni^{2+} ion prefer to octahedral site available in literatures[15-17], this cation distribution over the tetrahedral and octahedral sites for present systems are derived from X-ray Diffraction data. In present case the variation in coercivity is due to a rearrangement of Ni^{2+} and Mg^{2+} cations between octahedral to tetrahedral sublattices [18].

Table 3. Magnetic properties, Coercivity (Hc), Retentivity(Mr) and Cation distribution of Ni^{2+} and Mg^{2+} ions

Sr. No.	Compound	Saturation magnetization (Ms)	Retentivity (M_r) (emu/g)	Coercivity(H_c) (Gauss)	SQR Ratio Mr / Ms	Anisotropy Constant (K)
1	$Ni_{0.1}Mg_{0.9}Fe_2O_4$	0.1653	0.0216	165.58	0.13	$0.027x10^3$
2	$Ni_{0.15}Mg_{0.85}Fe_2O_4$	0.1742	0.0253	171.58	0.14	$0.030x10^3$
3	$Ni_{0.2}Mg_{0.8}Fe_2O_4$	0.4109	0.0758	167.16	0.18	$0.070x10^3$
4	$Ni_{0.25}Mg_{0.75}Fe_2O_4$	0.4171	0.0758	169	0.18	$0.071x10^3$
5	$Ni_{0.3}Mg_{0.7}Fe_2O_4$	0.3005	0.0660	171.44	0.21	$0.052x10^3$

From cation distribution of Ni^{2+} and Mg^{2+} ions on A and B site acquire magnetic moment on present system $Ni_xMg_{1-x}Fe_20_4$ this distribution are shown in table 4.

The proposed cation distribution is based on the fact that the Ni $^{2+}$ occupy in octahedral [B] site whereas Fe can occupy both tetrahedral and octahedral sites and Mg^{2+} give more preference to octahedral site.

Table4. Cation distribution of Ni , Mg and Fe cations on tetrahedral and octahedral sites

Sr. no.	concentration	Cation distribution of
1	X=0.1	$Mg_{0.341}Fe_{0.422})_{Tet.}[Ni_{0.1}Mg_{0.559}Fe_{1.578}]_{Oct.}$.
2	X=0.15	$(Mg_{0.344}Fe_{0.42})_{Tet.}[Ni_{0.15}Mg_{0.506}Fe_{1.58}]_{Oct}$
3	X=0.2	$(Mg_{0.347}Fe_{0.414})_{Tet.}[Ni_{0.2}Mg_{0.453}Fe_{1.586}]_{Oct.}$
4	X=0.25	$(Mg_{0.35}Fe_{0.41})_{Tet.}[Ni_{0.25}Mg_{0.4}Fe_{1.59}]_{Oct.}$
5	X=0.3	$(Mg_{0.352}Fe_{0.405})_{Tet.}[Ni_{0.3}Mg_{0.348}Fe_{1.595}]_{Oct}$

III. CONCLUSION

Ni substituted Magnesium Spinel ferrites (NixMg1-xFe2O4, 0<x,0.35) was prepared by the sol-gel auto combustion method. X-ray diffraction conform the formation of cubic spinel structure, X-rd Patterns reveal non-monotonical increase crystallite size in the range 23-32 nm, this variation in crystalline size is due to the decrease in strain and dislocation constant.

The hoping length L_A and L_B decreases with the substitution of Ni^{2+} ions in Spinel Ferrites. The average particles size acquire using histogram of High resolution TEM images manifest nearly the same particle size obtained from XRD data. FTIR spectrum shows the presence of tetrahedral and octahedral vibrational frequency ($\nu_1$and ν_2) and force constant Kt and Ko. Also it shows the cation distribution of Ni^{2+} and Mg^{2+} ions on tetrahedral and octahedral sites effects the magnetic property like Coercivity and retentivity.

All this properties follow the formation of cubic spinel ferrites with nanostructures. These nanostructure ferrites are useful in biomedical applications.

REFERENCES

[1] A. Baykal, I.A. Auwal, S. Güner, H. Sözeri, "Magnetic and optical properties of Zn^{2+} ion substituted barium hexaferrites" J. Magn. Magn. Mater., 430 **(2017)** 29–35.

[2] S. Güner, A. Baykal, Md. Amir, H. Güngüneş, M. Geleri, H. Sözeri, Sagar E. Shirsath, M. Sertkol,"Synthesis and characterization of oleylamine capped $Mn_xFe_{1-x}Fe_2O_4$ nanocomposite: Magneto-optical properties, cation distribution and hyperfine interactions", J. Alloys Compds., 688 **(2016)** 675–686.

[3] C.O. Ehi-Eromosele1*, J.A.O. Olugbuyiro1*, O.S. Taiwo2, O.A. Bamgboye1 and C.E. Ango "Synthesis And Evaluation Of The Antimicrobial Potentials Of Cobalt Doped-And Magnesium Ferrite Spinel Nanoparticles" Bull. Chem. Soc. Ethiop. (**2018)**, 32(3), 451-458.

[4] H. Bahiraeia, C.K. Ong, "Microstructural and electromagnetic study of low temperature fired nano crystalline MgCuZn ferrite with Bi_2O_3" Ceram. Int. 43 **(2017)** 4780–4784.

[5] A. Godlyn Abraham, A. Manikandan, E. Manikandan, S. Vadivel, S.K.Jaganathan, A. Baykal, P. Sri Renganathan "Enhanced magneto-optical and photo-catalytic properties of transition metal cobalt (Co^{2+} ions) doped spinel $MgFe_2O_4$ ferrite nanocomposites" *Journal of Magnetism and Magnetic Materials"* **(2018)** doi: https://doi.org/10.1016/j.jmmm.2018.01.001

[6] P. Chirawatkul, S. Khoonsap, S. Poomying, C. Kaewhan, S. Pinitsoontorn, S. Maensiri, "Cation distribution and magnetic properties of $Co_xMg_{1-x}Fe_2O_4$ Nanoparticles", *Journal of Alloys and Compounds* **(2017)** doi: 0.1016/j.jallcom.2016.12.106

[7] L. Sun, R. Zhang, Q. Ni, E. Cao, W. Hao, Y. Zhang, L. Ju, "Magnetic and dielectric properties of $Mg_xCo_{1-x}Fe_2O_4$ ferrites prepared by the sol-gel method", *Physica B: Physics of Condensed Matter* **(2018),** doi: 10.1016/j.physb.2018.05.030

[8] Xiqian Zhao, Aimin Sun; Wei Zhang, Lichao Yu, Zhuo Zuo, Nanzhaxi Suo, Xiaoguang Pan; and Yingqiang Han "Studies on structural and magnetic properties of Ni-Mg-Co spinel ferrite nanoparticles sintered at different temperatures" Modern Physics Letters B Vol. 34, No. 3 (2020) 2050041 DOI: 10.1142/S0217984920500414.

[9] P. Samoila, L. Sacarescu, A.I. Borhan, D. Timpu, M. Grigoras,N. Lupu, M. Zaltariov, V. Harabagiu,"Magnetic Properties of nanosized Gd doped Ni-Mn-Cr ferrites prepared using the sol-gel autocombustion technique.Journal of Magn. Magn Mater**. 378**,92–97 **(2015)**

[10] Shaik Jesus Mercy, N. Murali A. Ramakrishna Y. Ramakrishna V. Veeraiah K. Samatha "Microstructural, thermal, electrical and magnetic analysis of Mg^{2+}substituted Cobalt ferrite" Applied Physics A **(2020)** 126:873 https://doi.org/10.1007/s00339-020-04048-6

[11] Y. Slimania, M.A. Almessierea, M. Sertkolc, Sagar E. Shirsathd, A. Baykale, M. Nawaze,S. Akhtara, B. Ozcelikf, I. Ercana "Structural, magnetic, optical properties and cation distribution of nanosized $Ni_{0.3}Cu_{0.3}Zn_{0.4}Tm_xFe_{2-x}O_4$ ($0.0 \leq x \leq 0.10$) spinel ferrites synthesized by ultrasound irradiation" Ultrasonics - Sonochemistry 57 (2019) 203–211

[12] Waldron RD Infrared spectra of ferrites. Phys Rev 99: **(1955)** 1727–1735.

[13] P.S. Hedaoo, D.S. Badwaik, K.G. Rewatkar "Structural and Magnetic Studies of Zn Doped Nickel Nanoferrites Synthesize by Sol-gel Auto Combustion Method" materials today 15(2019)416-423.

[14] A. S. Kakde, D. M. Borikar, K. G. Rewatkar " Nickel nano spinel ferrites: synthesis and characterization" International Conference on Electrical, Electronics, and Optimization Techniques (ICEEOT) - 2016

[15] Cullity B.D., Elements of X-ray Diffraction, Addison-Wesley Publishing Company, Massachusetts,**1978**

[16] Mohammed K.A., Al-Rawas A.D., Gismelseeda.M., Sellai A., Widatallah H.M., Yousif A.,Elzain M.E., Shongwe M., Physica B, 407, **(2012),**795.

[17] B.B.V.S. Vara Prasad, B. Rajesh Babu, M. Siva Ram Prasad "Structural and dielectric studies of Mg^{2+} substituted Ni–Zn ferrite" Materials Science-Poland, 33(4), **(2015),** pp. 806-815

[18] K. Ramarao, B. Rajesh Babu, B. Kishore Babu, V. Veeraiah, K. Rajasekhar, B. Ranjith Kumar4, B. Swarna Latha "Enhancement in magnetic and electrical properties of Ni substituted Mg ferrite." Materials Science-Poland, 36(4),**(2018),** pp. 644-654.